

# Predicting Gradient is Better: Exploring Self-Supervised Learning for SAR ATR with a Joint-Embedding Predictive Architecture

Weijie Li<sup>a</sup>, Wei Yang<sup>a,\*</sup>, Tianpeng Liu<sup>a</sup>, Yuenan Hou<sup>b</sup>, Yuxuan Li<sup>c</sup>, Zhen Liu<sup>a</sup>, Yongxiang Liu<sup>a,\*</sup> and Li Liu<sup>a,\*</sup>

<sup>a</sup>the College of Electronic Science and Technology, National University of Defense Technology, Changsha, 410073, China

<sup>b</sup>the Shanghai AI Laboratory, Shanghai, 200000, China

<sup>c</sup>the Visual Computing and Intelligent Perception Lab, Nankai University, Tianjin, 300071, China

## ARTICLE INFO

### Keywords:

Synthetic Aperture Radar (SAR)  
Automatic Target Recognition (ATR)  
Self-Supervised Learning (SSL)  
Deep Learning  
Masked Image Modeling (MIM)

## ABSTRACT

The growing Synthetic Aperture Radar (SAR) data has the potential to build a foundation model through Self-Supervised Learning (SSL) methods, which can achieve various SAR Automatic Target Recognition (ATR) tasks with pre-training in large-scale unlabeled data and fine-tuning in small labeled samples. SSL aims to construct supervision signals directly from the data, which minimizes the need for expensive expert annotation and maximizes the use of the expanding data pool for a foundational model. This study investigates an effective SSL method for SAR ATR, which can pave the way for a foundation model in SAR ATR. The primary obstacles faced in SSL for SAR ATR are the small targets in remote sensing and speckle noise in SAR images, corresponding to the SSL approach and signals. To overcome these challenges, we present a novel Joint-Embedding Predictive Architecture for SAR ATR (SAR-JEPA), which leverages local masked patches to predict the multi-scale SAR gradient representations of unseen context. The key aspect of SAR-JEPA is integrating SAR domain features to ensure high-quality self-supervised signals as target features. Besides, we employ local masks and multi-scale features to accommodate the various small targets in remote sensing. By fine-tuning and evaluating our framework on three target recognition datasets (vehicle, ship, and aircraft) with four other datasets as pre-training, we demonstrate its outperformance over other SSL methods and its effectiveness with increasing SAR data. This study showcases the potential of SSL for SAR target recognition across diverse targets, scenes, and sensors.

## 1. Introduction

Synthetic aperture radar (SAR) possesses the capability to capture images under diverse weather and lighting conditions, rendering it indispensable for acquiring Earth observation information (Sun et al., 2021; Moreira et al., 2013; Tsokas et al., 2022). As a crucial component in SAR image interpretation, SAR Automatic Target Recognition (ATR) aims to localize and classify desired targets within SAR images. Over the past few decades, extensive research has been conducted in this field with various civilian and military applications, including transportation management (Gagliardi et al., 2023), autonomous driving (Rizzi et al., 2021), and military surveillance (Li et al., 2023b; Peng et al., 2022). Deep learning has revitalized SAR ATR in the last decade with remarkable advancements (Kechagias-Stamatis and Aouf, 2021; Li et al., 2023a; Datcu et al., 2023). Despite significant progress, the high costs of data collection and annotation limit dataset diversity and method applications. SAR ATR studies are categorized into subfields such as

vehicle (Li et al., 2023b), ship (Hou et al., 2020), and aircraft recognition (Zhao et al., 2022) with many specialized approaches. Hence, an intriguing and worthwhile question to explore is *whether a generic representation and method exist for various SAR target recognition tasks*.

The emerging self-supervised learning techniques present a potential solution to this question. Self-supervised learning (SSL) aims to extract meaningful signals directly from the data, thereby reducing the need for costly expert annotations and efficiently using the growing number of data. Foundation models, which are trained on extensive datasets using SSL, have demonstrated their effectiveness in various computer vision (Goldblum et al., 2023; He et al., 2022), remote sensing (Sun et al., 2023), and clinical medical tasks (Zhou et al., 2023b). Therefore, we believe that foundation models, trained through SSL on a large dataset, can yield a generalized representation for SAR target recognition. With this aim, this paper investigates the key challenges in SSL for SAR ATR.

**Lack of a large-scale pre-training set.** Just as ImageNet (Fei-Fei and Krishna, 2022) has achieved an impressive contribution to computer vision by pushing the number of categories for object recognition from twenty to thousands, a large-scale pre-training set for SAR target recognition will bring new research ideas and tasks. Unfortunately, due to the acquisition cost and annotation difficulties, many SAR target datasets have at most ten annotation categories and a few thousand images. Whereas some studies (Huang et al., 2022; Zhai et al., 2022; Pei et al., 2023) in SAR target

\*This document was supported by the National Key Research and Development Program of China (No. 2021YFB3100800), the National Natural Science Foundation of China (No. 61871384, 61901487, 61901498, and 61921001), and the Science and Technology Innovation Program of Hunan Province (No. 2022RC1092).

\*Corresponding author: Li Liu, wei Yang, and Yongxiang Liu

✉ lwj2150508321@sina.com (W. Li); yw850716@sina.com (W. Yang);  
everliutianpeng@sina.cn (T. Liu); houyuenan@pjlab.org.cn (Y. Hou);  
yuxuan.li.17@ucl.ac.uk (Y. Li); zhen\_liu@nudt.edu.cn (Z. Liu);  
lyx\_bible@sina.com (Y. Liu); dreamliu2010@gmail.com (L. Liu)

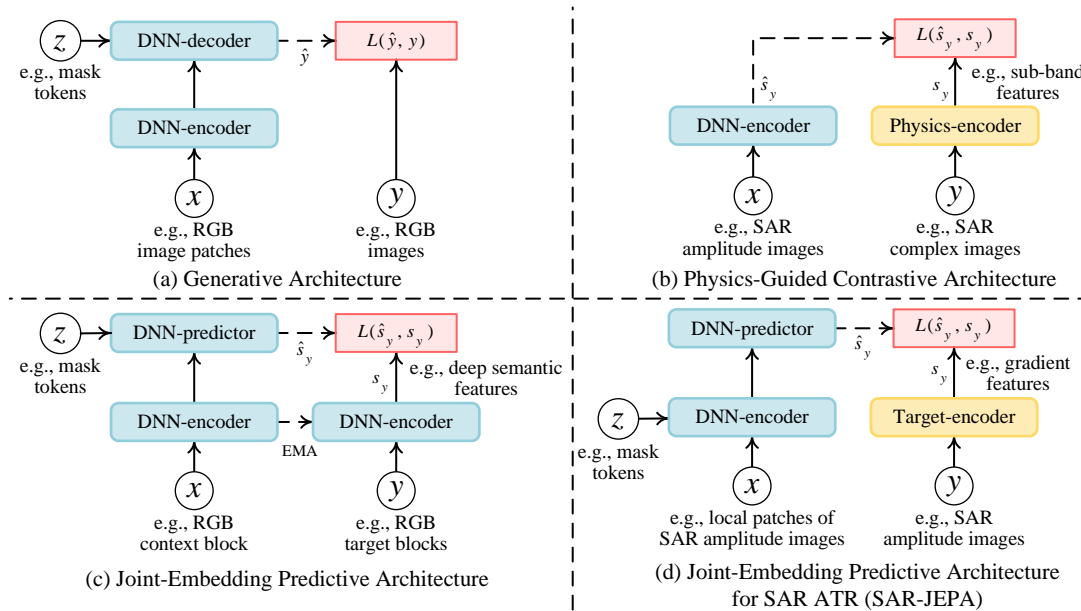


**Figure 1:** Comparison of related architectures and the proposed architecture. (a) Generative architectures (He et al., 2022) focus on reconstructing the pixels of unseen patches with a high mask proportion. This approach creates a challenging and meaningful pretext task that allows the model to learn contextual relationships within images. (b) Physics-guided contrastive architectures (PGCA) (Datcu et al., 2023; Huang et al., 2022) leverage the unique representation in the SAR domain as guided signals to constrain the representation of the Deep Neural Network (DNN). By incorporating physical principles into the learning process, PGCA enhances the model’s ability to capture accurate and important SAR features. (c) Joint-Embedding Predictive Architecture (I-JEPA) (Assran et al., 2023) use deep features as target signals and learn more semantic information. However, we found that a learnable target encoder is susceptible to feature collapses due to SAR image noise. (d) Our Joint-Embedding Predictive Architecture for SAR ATR (SAR-JEPA) combines SAR domain embedding and the meaningful MIM pretext task to learn contextual relationships in the SAR gradient feature space. This approach utilizes prior knowledge about SAR target recognition in target scale and features to improve the representation.

recognition used a few datasets as pre-training and evaluations, the potential of self-supervised learning in large-scale SAR datasets has yet to be explored fully. Therefore, it is necessary to integrate increasing open-source datasets to construct a large-scale pre-training set containing diverse targets, scenes, and sensors<sup>1</sup>.

**Special properties of SAR images.** SAR achieves coherent imaging through a moving platform in remote sensing. Its images reflect the electromagnetic scattering of objects, but they are often affected by multiplicative speckle noise, phase errors, and other interferences. Consequently, SAR image interpretation is extremely difficult and poses difficulties for SSL methods due to unique imaging properties. Our study focuses on addressing two key issues: the scale problem and target features. Firstly, remote sensing images often contain large scenes and small targets, making it difficult to learn effective contextual information for various targets. Current pre-training methods for SAR target recognition focus less on this issue because they have mainly focused on a few datasets that lack significant scale problems in the dataset. Secondly, SAR images are affected by speckle noise, which can impact the quality of learned

<sup>1</sup>Various imaging conditions regarding target, scene, and sensor can lead to complex target and background signature variations in SAR images (Ross et al., 1999; Li et al., 2023b).

representations. This issue was addressed through data augmentation (Zhai et al., 2022) and filtering methods (Pei et al., 2023) in contrastive SSL, as well as Histogram of Oriented Gradients (HOG) features (Wang et al., 2023d) in generative SSL. However, data augmentation in contrastive learning can not simulate the effects of speckle noise exactly, and the gradient computation in HOG features has false results due to multiplicative noise. Based on the above discussions, these two issues still require adequate solutions. We aim to leverage SAR domain knowledge to address these unique challenges for SSL in pretext tasks and target signals.

In order to deploy SSL for SAR ATR, we first constructed a pre-training dataset consisting of approximately 100,000 SAR magnitude images sourced from four open-source datasets (Xia et al., 2022; Chen et al., 2022b; Wang et al., 2019; Malmgren-Hansen et al., 2017; Kusk et al., 2016; Lewis et al., 2019). This pre-training dataset encompasses a wide range of target categories, scenes, and sensors, allowing us to explore effective SSL methods. To address the abovementioned issues, we proposed a novel Joint-Embedding Predictive Architecture for SAR ATR (SAR-JEPA<sup>2</sup>) in Figure 1. SAR-JEPA leverages gradient embedding and the Masked Image Modeling (MIM) task to learn contextual relationships within the SAR feature space.

<sup>2</sup>Our codes and weights: <https://github.com/waterdisappear/SAR-JEPA>

We employed the well-established Gradient-by-Ratio (GR) method (Dellinger et al., 2014; Song et al., 2016) as target feature, effectively mitigating the impact of speckle noise in SAR images and facilitating accurate target shape extraction. Furthermore, we introduced local masks and multi-scale features to enhance the architecture’s adaptability to various small target scales in remote sensing. To evaluate the effectiveness of our proposed architecture, we conducted experiments on three datasets (vehicle, ship, and aircraft).

Numerous experiment results demonstrate that SAR-JEPA achieves improved performance than other SSL methods. Importantly, it can increase with the volume of pre-training data, thereby showing the potential of SSL to build a foundation model to unify SAR ATR across different targets, scenes, and sensors. In summary, the main contributions of this article are as follows:

- We construct comprehensive SAR pre-training and fine-tuning settings to study SSL for SAR ATR self-supervised learning. A novel joint-embedding predictive architecture for SAR ATR (SAR-JEPA) is proposed to learn contextual relationships within the SAR gradient feature space.
- The core of SAR-JEPA lies in the self-supervised learning method and the target feature construction. SAR-JEPA learns contextual information around small targets in remote sensing images more efficiently by local masking. SAR-JEPA uses multi-scale gradient features as guidance signals to solve SAR speckle noise interference.
- SAR-JEPA’s performance with increasing data volume demonstrates the potential of SSL to learn generalized feature representations. We hope it will stimulate the enthusiasm for research on fundamental models of SAR target recognition.

The remainder of this paper is organized as follows. Sec. 2 introduces related studies in SSL. Sec. 3 introduces the proposed SAR-JEPA. Sec. 4 conducts extensive experiments and analyses for the effectiveness and scaling capabilities of our architecture. Sec. 5 concludes the whole paper and discusses future work.

## 2. Related Work

### 2.1. Self-supervised learning in computer vision

Self-supervised learning (Liu et al., 2021; Balestriero et al., 2023) aims to learn the intrinsic relationship in samples through a pretext task. This method can leverage a huge amount of unlabelled data and perform well in various downstream tasks. Self-supervised learning methods can be broadly categorized into contrastive and generative approaches (Liu et al., 2021). In this study, we focus on generative masked image modeling because it can model both local and long-range information (Xie et al., 2023b), and the data augmentation pretext task in the contrastive approach is not fully compatible with the SAR image properties. BEiT (Bao et al., 2021) proposed the concept of

masked image modeling and predicted the masked patches in a frozen pre-training tokenized space. Compared to BEiT, MAE (He et al., 2022) achieved an efficient and meaningful task through asymmetric autoencoder structure and high masking rate. Furthermore, SimMIM (Xie et al., 2022) showed that masked image modeling can be achieved with a simple structure, such as a linear projection layer and a random mask. Over time, a series of improvement works have emerged, and our focus is on research in masking methods and target features.

**Masking strategy** can affect the representation quality, which is centered on ensuring pretext task difficulty and learning contextual information around target regions. MAE (He et al., 2022) and SimMIM (Xie et al., 2022) compared different sampling strategies, such as random sampling, block sampling, and grid sampling, and found that random sampling with a large mask ratio works best. I-JEPA (Assran et al., 2023) employed block sampling and used a single context block to predict several non-overlapping target blocks to exploit the rich semantics in the context block. Hard patches mining (Wang et al., 2023b) applied a teacher network to predict the reconstruction loss of different patches to better mine the target foreground region. PixMIM (Liu et al., 2023) used a simple random resized crop to preserve more of the target foreground region in the random mask for semantic concept learning. Inspired by the fact that target reconstruction in MAE mainly uses the surrounding area, Local Masked Reconstruction (LoMaR) (Chen et al., 2022a) proposed to perform masked reconstruction within a local image block instead of the whole image to improve computational efficiency. As for remote sensing images, the masking strategy must consider their large scene and small target properties. We applied the LoMaR method to learn local contextual information.

**Target features.** Masked image modeling learns contextual information by reconstructing and predicting various feature representations, such as pixel values (He et al., 2022; Xie et al., 2022), discrete tokens (Bao et al., 2021), HOG features (Wei et al., 2022; Wang et al., 2023c), deep features (Wei et al., 2022; Assran et al., 2023), and frequency features (Xie et al., 2023a; Liu et al., 2023). MaskFeat (Wei et al., 2022) proved that the target features can be either the classical HOG feature or deep features obtained by other self-supervised methods. LocalMIM (Wang et al., 2023c) performed multiscale reconstruction of HOG features at different encoder layers to facilitate representation learning speed and semantic understanding of scales. I-JEPA (Assran et al., 2023) used a learnable target encoder to get deep semantic features. PixMIM (Liu et al., 2023) enhanced the learning of low-frequency components such as target shape by reconstructing the image after low-pass filtering. Masked frequency modeling (Xie et al., 2023a) avoided spatially redundant masking by reconstructing different frequency components. A priori knowledge can be incorporated as a target feature to guide representation learning. In particular, our SAR-JEPA is inspired by the architecture of I-JEPA, which uses a learnable target encoder to learn deep semantic

information. However, we found that this approach leads to feature collapse with SAR image noise. Therefore, we used the gradient-by-ratio method in SAR to extract the target edge shape features and suppress the speckle noise.

## 2.2. Self-supervised learning in remote sensing

In recent years, there has been a growing interest in self-supervised learning for remote sensing, which provides a paradigm for solving the contradiction between increasing samples and the lack of high-quality annotations (Wang et al., 2022b). Self-supervised learning has many applications in multi-source data such as multispectral (Reed et al., 2023; Sun et al., 2023), hyperspectral (Ibanez et al., 2022), and SAR (Wang et al., 2023d; Huang et al., 2022; Zhai et al., 2022) with various paradigms of contrastive and generative.

Due to the lack of a large-scale dataset, self-supervised learning in SAR ATR is relatively scarce (Zhai et al., 2022; Pei et al., 2023; Li et al., 2023b; Wen et al., 2021). These studies rely on contrastive learning or target rotation angle information. However, data augmentation methods applied on natural images may not be fully suitable for SAR images (Wang et al., 2022b). For example, Gaussian blurring and noise methods can not simulate multiplicative speckle noise effects, and the rotation is incompatible with SAR images because of the anisotropic electromagnetic scattering. In addition, only a few datasets provide information on the target rotation angle. Compared to applying multiple data augmentation methods to simulate the imaging condition variations and noise interference for SAR images (Zhai et al., 2022; Pei et al., 2023; Li et al., 2023b), we prefer another contrastive architecture (Datcu et al., 2023) compatible with SAR images' properties. Its contrastive architecture used SAR domain features to guide representation learning. We combine this idea with MIM to learn contextual semantic information within the feature space. And the target features with the SAR image properties can ensure a high-quality representation. We discuss self-supervised learning in remote sensing and SAR from three aspects.

**Pre-train dataset.** There is no unified benchmark setting for self-supervised learning with SAR target recognition due to the lack of a large dataset such as ImageNet. For scene classification (Wang et al., 2023d; Huang et al., 2022), the pre-training sets used BigEarthNet-MM (Sumbul et al., 2021) or the sea ice dataset (Huang et al., 2022). For target recognition (Zhai et al., 2022; Pei et al., 2023), the pre-training sets applied the MSTAR vehicle (Air Force Research Laboratory) or OpenSAR ship (Huang et al., 2017) datasets. Previous work for SAR target recognition (Zhai et al., 2022; Pei et al., 2023) used pre-training sets that contain several target categories and scenarios. Therefore, the potential of self-supervised learning for foundation models in SAR target recognition has yet to be investigated. Constructing a more large dataset containing various targets, scenes, and sensors is necessary.

**Scale of target and scene.** A major difference between remote sensing and computer vision is in scene range and target size. Remote sensing images usually contain large

scenes and small targets (Li et al., 2023c; Cheng et al., 2023). TOV (Tao et al., 2023) illustrated that small scenes with different semantics within a larger scene affect contrastive learning. Chen et al. (Chen and Bruzzone, 2022) used shift alignment of two local regions between SAR and optical images in contrast learning. RingMo (Sun et al., 2023) proposed a PIMask sampling strategy for dense small targets in remote sensing images, *i.e.*, secondary pixel sampling of the masked patches to expose small targets. However, we found that pixel sampling does not work for SAR images because the single pixels of SAR images contain multiplicative noise. Therefore, we prefer local patches for masking instead of the whole image or pixel level.

**SAR speckle noise.** Speckle noise affects the quality of self-supervised learning features, so the researcher has used many ways, such as data augmentation (Zhai et al., 2022), filtering (Pei et al., 2023), and feature extraction, to address the problem. Zhai et al. (Zhai et al., 2022) added Gaussian noise and blur to data augmentation methods. But Gaussian noise and blurring do not perfectly match multiplicative speckle noise. Pei et al. (Pei et al., 2023) used the despeckling pre-processing method in contrastive learning to address speckle noise. We focus on extracting high-quality features as guide signals, which accomplish noise reduction and feature extraction. Similarly to our work, Wang et al. (Wang et al., 2023d) discussed different features such as CannyEdge (Canny, 1986), HOG, and SAR-SIFT (Dellinger et al., 2014) features for SAR scene classification and segmentation. They found HOG is more appropriate than SAR-SIFT for SAR SSL. Our work aims to mine semantic information at the target level rather than the scene level through local patches, and we found that gradient-by-ratio is more suitable for target shape information extraction than HOG's differential gradient under multiplicative speckle noise.

## 3. Approach

The proposed Joint-Embedding Predictive Architecture for SAR target recognition (SAR-JEPA) is illustrated in Figure 2. Our overall objective is as follows: given local masked patches, predict feature representations in the SAR domain, *w.r.t.*, the model can achieve SAR image interpretation by recognizing the contextual relationship between the target parts and the surrounding area.

As shown in Figure 2, the input is the single-channel SAR magnitude image since most target datasets are magnitude pictures. We randomly select different local patches and add mask tokens according to LoMaR (Chen et al., 2022a). Vision Transformers (ViT) (Dosovitskiy et al., 2020) in MAE are used as the DNN-encoder and DNN-predictor. Each local masked patch is fed into the MIM structure to predict the target feature of mask tokens. Importantly, the special SAR coherent imaging mechanism requires predicting high-quality target features instead of noisy pixels. SAR coherent imaging results in multiplicative speckle noise in the magnitude image, and we use the gradient-by-ratio (Dellinger et al., 2014; Song et al., 2016) to suppress

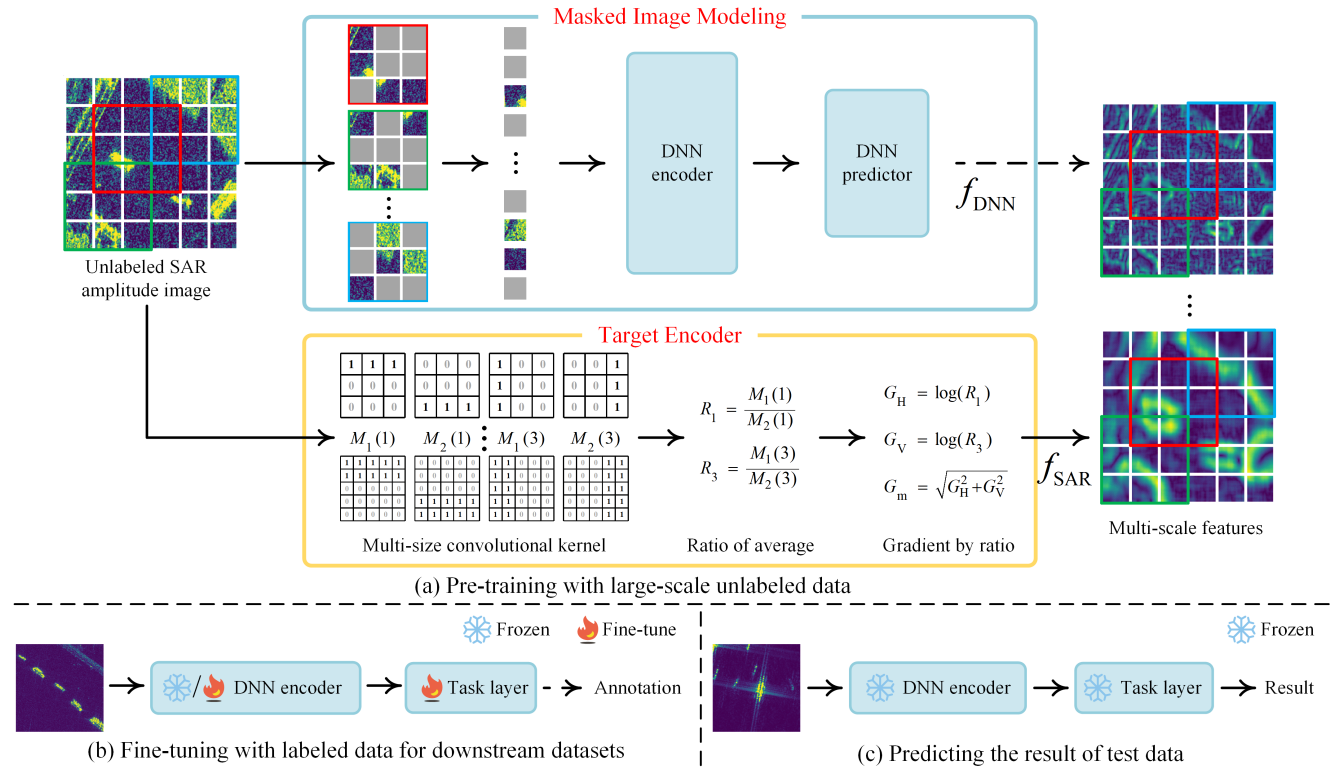


**Figure 2:** The overall framework of SAR-JEPA. (a) In the pre-training stage, our Joint-Embedding Predictive Architecture for SAR target recognition (SAR-JEPA) uses local masked patches to predict the multi-scale SAR feature representations  $f_{\text{SAR}}$  of unseen patches. The MIM structure uses the Vision Transformer (ViT) in MAE and extracts deep features  $f_{\text{Deep}}$  of masked patches. Its DNN predictor predicts SAR features of unseen patches. The target encoder uses the gradient-by-ratio method to map SAR images from pixel to feature space, thus extracting the target shapes and avoiding speckle noise interference in SAR images. Local patches and multi-scale features are designed for multi-scale small targets in remote sensing. For downstream datasets, we fine-tune the DNN encoder with a task layer using labeled training data. DNN encoder weights are frozen or fine-tuned using different tuning settings. Other model module weights are dropped. (c) The trained model is used to predict the test result.

noise and extract the targets' edge and shape. Moreover, we employ a multi-scale and local mask setting for various targets in the pre-training set.

### 3.1. Local Masked Patches

We aim to learn the contextual relationship of various targets. However, such relationships normally remain in small areas due to the large scale and small target in remote sensing imagery. Therefore, we perform masking in the local patches following LoMaR. Although LoMaR is designed to improve computational efficiency, we found this local setting is suited for small targets in remote sensing. According to the LoMaR, mask tokens and relative positional encoding (Wu et al., 2021) are added to the encoder input and MAE structure to enhance the feature representation. These are important for LoMaR to avoid feature collapse.

### 3.2. Target Encoder

Due to the SAR imaging mechanism (Moreira et al., 2013), the images' amplitude values contain multiplicative speckle noise. The speckle noise is related to the sensor resolution and is caused by the coherent superposition of

different scatterers within a scattering cell. Therefore, reconstructing image pixels for SAR images receives noise interference and fails to learn a high-quality feature representation. This problem of speckle noise can be solved by filtering and feature extraction. However, filtering has a conflict between noise reduction and image details, and we use feature extraction. Some studies have proposed different types of target features in computer vision, mainly divided into traditional manual features (Wei et al., 2022) and deep learning features (Assran et al., 2023). However, these methods are difficult to migrate to SAR target recognition directly, and we combine the well-established local description feature methods (Dellinger et al., 2014; Song et al., 2016; Dong et al., 2020) in the SAR domain.

**Gradient computation.** The differential gradient is not a constant false alarm rate operator due to multiplicative speckle noise in the SAR image, and previous studies (Touzi et al., 1988; Bovik, 1988) have shown that the computing ratio is more suitable for multiplicative noise. Here, we use the simplest ratio of average (ROA) (Touzi et al., 1988) so as not to blur image details:

$$R_i = \frac{M_1(i)}{M_2(i)}, \quad (1)$$

where  $R_i$  denotes the average ratio at different directions and  $M_1(i)$  and  $M_2(i)$  are the area averages on opposite sides of the current pixel along direction  $i$ .  $i = 1$  is the horizontal direction and  $i = 3$  means the vertical direction. As shown in Figure 2, the area averages  $M$  can be computed from the input image with four fixed convolution kernels<sup>3</sup>. Each convolution kernel extracts the sum of the region on one side of the pixel point, which is averaged to obtain  $M$ . By varying the size of the convolution kernel, the multi-scale features  $f_{\text{SAR}}$  can be obtained.

Then, the use of logarithms can solve the vertical gradient calculation (Dellinger et al., 2014), and the horizontal and vertical gradients are defined as:

$$\begin{aligned} G_H &= \log(R_1) \\ G_V &= \log(R_3) \end{aligned} \quad (2)$$

where  $G_H$  is the horizontal gradient and  $G_V$  is the vertical gradient. The gradient magnitude is  $G_m = \sqrt{G_H^2 + G_V^2}$ . We use gradient magnitude to construct multi-scale gradient features  $f_{\text{SAR}}$ .

**Multi-Scale Feature.** SAR-HOG (Song et al., 2016) has discussed the kernel sizes for SAR vehicle target recognition and given the best single size for the MSTAR vehicle dataset. However, a single-size kernel cannot accommodate various targets when the dataset is extended to different targets and sensors. Due to the dynamic range of contextual information for various targets in remote sensing (Li et al., 2023c), a multi-scale feature is constructed with convolutional kernels of different sizes in Figure 1.

We set the kernel size  $r$  equal to 5, 7, 13, and 17, and the whole convolution kernel is a square with an odd  $2r + 1$ . Though different kernel sizes, we have four gradient features  $G_{m1}$ ,  $G_{m2}$ ,  $G_{m3}$ , and  $G_{m4}$ , and the multi-scale feature  $f_{\text{SAR}} = \text{cat}(G_{m1}, G_{m2}, G_{m3}, G_{m4})$  is a concatenation of four gradient features in the feature channel. As shown in Figure 1, small-scale convolution kernels provide a finer extraction of small target contours, while large-scale convolution kernels focus on large targets and scene edges and noise suppression.

### 3.3. Implementation

Given SAR images, we randomly sample several square windows at different spatial locations as local patches and mask each patch with mask tokens at a fixed percentage. Then, each local masked patch's visible and unseen parts are fed into the MIM structure, whose encoder and predictor are applied with learnable relative positional encoding in the self-attention layer. Meanwhile, the whole SAR image is provided to the target encoder. The average values in four directions are obtained after multi-scale convolution in four directions. Then, the multi-scale SAR features are obtained after the ratio, logarithm, and magnitude operations. The loss function computes the mean squared error in the feature space between the DNN features  $f_{\text{Deep}}$  and SAR multi-scale features  $f_{\text{SAR}}$  for masked patches. In addition to the major improvement of the target encoder, there are two other minor.

<sup>3</sup>We added  $1e-2$  to the input image to prevent zero values.

**Data augmentation.** We follow the simple data augmentations in MAE and add a random contrast adjustment for SAR magnitude images.

**Decoder design.** While some work (Chen et al., 2022a; Wei et al., 2022) has shown that it is feasible to use a simple linear head as a decoder or predictor for self-supervised learning in RGB images, we find that a ViT with eight-layers in the MAE is less disturbed by SAR image noise than a linear layer, allowing the encoder to extract deep semantic features of targets.

## 4. Experiments

This section analyzed the proposed architecture. We first described the pre-training and few-shot classification experimental setting in Sec. 4.1. Then, we discussed the effectiveness of the different modules in our architecture in Sec. 4.2. And the proposed SAR-JEPA was compared with other methods in Sec. 4.3 and in Sec. 4.4. In the end, Sec. 4.5 discussed the scaling experiment and SAR-JEPA showed improved performance with increasing unlabeled data.

### 4.1. Dataset and Experimental Settings

We examine self-supervised learning performance with the following procedure. First, we perform the self-supervised learning on the pre-training dataset without label information. Then, we fine-tune the pretrained model on few-shot SAR classification datasets.

**Pre-training.** Pre-training datasets are designed to ensure rich information about targets, scenes, and sensors. Therefore, we chose four datasets to build a pre-training dataset for SSL. It covers popular targets (vehicles, ships, aircraft, etc.), complex backgrounds (ground and ocean), and various sensors (satellite-borne, airplane-borne, and simulation) in Table 1 and Figure 3.

MSAR (Xia et al., 2022; Chen et al., 2022b) is a multi-class target detection dataset based on the Chinese HISEA-1 satellite in large-scale scenes. MSAR comprises 28,449 image slices with quad polarization. Scenes covered include airports, harbors, nearshore, islands, distant seas, urban areas, etc. The labeled target categories include aircraft, oil tanks, bridges, and ships. This dataset can provide target samples in complex ground and sea scenes.

SAR-Ship (Wang et al., 2019) dataset is a ship detection dataset in complex scenes based on Chinese Gaofen-3 and European Sentinel-1 satellites. The public version of this dataset contains 39,729 images from two satellites in different imaging modes and resolutions. The dataset provides ship targets of various sizes in complex ocean scenes such as nearshore, distant seas, harbors, and islands.

SARSim (Malmgren-Hansen et al., 2017; Kusk et al., 2016) is a fine-grained vehicle dataset created by Terma A/S, Denmark. The simulation system used for this dataset can generate X-band SAR images with resolutions ranging from 0.1m to 0.3m from CAD models. SARSim provides 21,168 vehicle samples in 7 categories (truck, car, motorbike, bus, tank, bulldozer, and pickup) and 3 scenes (grass, roads, and

**Table 1**

Description of SAR datasets used for pre-training and downstream tasks. # Target: Number of target categories. # Scene: Number of scenes. Res.: Resolution. Large SAR imagery in the detection contains more target and scene types than the annotation.

Dataset	Size	# Target	# Scene	Res. (m)	Band	Polarization	Description
MSAR	28,499	$\geq 4$	$\geq 6$	1	C	Quad	Ground and sea targets detection dataset
SAR-Ship	39,729	$\geq 1$	$\geq 4$	3~25	C	Quad	Ship detection dataset in complex scenes
SARSim	21,168	7	3	0.3	X	Single	Vehicle simulation dataset
SAMPLE	5,380	10	1	0.3	X	Single	Vehicle simulation and measured dataset
MSTAR	5,216	10	1	0.3	X	Single	Fine-grained vehicle classification dataset
FUSAR-Ship	9,830	10	$\geq 5$	1.1~1.7	C	Double	Fine-grained ship classification dataset
SAR-ACD	2,537	6	3	1	C	Single	Fine-grained aircraft classification dataset

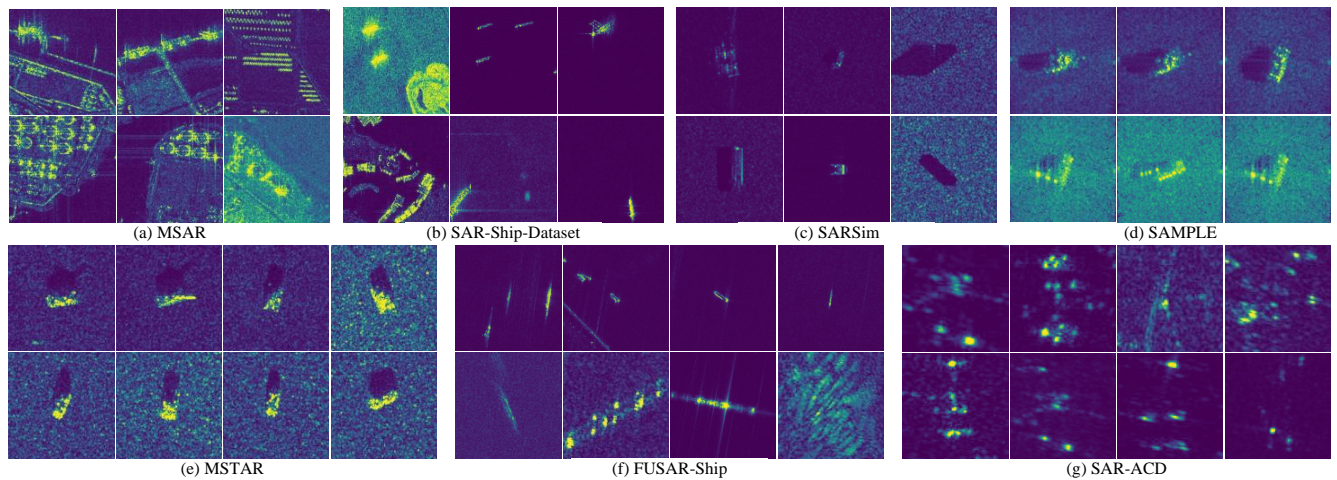


**Figure 3:** Datasets for the pre-training and downstream tasks. Pre-training contain different targets, scenes, and sensors from MSAR, SAR-Ship-Dataset, SARSim, and SAMPLE. MSAR is the satellite-based dataset of ground and sea targets; SAR-Ship-Dataset is the satellite-based dataset of sea targets; SARSim is the multi-angle simulation dataset of vehicle targets; and SAMPLE is the simulated and measured dataset of vehicle targets. We use MSTAR, FUSAR-Ship, and SAR-ACD datasets to evaluate the performance for recognizing different targets. MSTAR is a fine-grained vehicle dataset; FUSAR-Ship is a sea targets dataset; SAR-ACD is a fine-grained aircraft dataset.

a mean of the two) with 7 imaging depression angles. This dataset provides fine-grained differences between targets.

SAMPLE (Lewis et al., 2019) is a fine-grained synthetic and measured paired vehicle dataset released by the Air Force Research Laboratory, USA. This dataset is simulated in X-band and 0.3m resolution. The public version of this dataset provides 5,380 images of ten categories of military vehicle targets at partial imaging angles, and five categories overlap with the public version of MSTAR. As shown in Figure 3, it can be noticed that the ground clutter in SAMPLE is more significant and realistic than in SARSim.

**Downstream tasks.** We tested the pre-trained model on three target recognition datasets to evaluate the ability for fine-grained semantic classification in the case of small samples with fine-tuning and linear probing. According to MAE, fine-tuning is tuning all model parameters, and linear probing is tuning a linear layer with batch normalization while freezing other parameters.

MSTAR (Air Force Research Laboratory) is the most commonly used SAR target classification dataset released

by the Defense Advanced Research Projects Agency, USA, which contains ten categories of vehicles with different angles, variants, and other imaging conditions. It has many experimental setting variants, while we refer to the (Li et al., 2023b) to adopt the most commonly used ten-class classification settings to evaluate the fine-grained classification performance for SAR vehicles.

FUSAR-Ship (Sun et al., 2022) contains 15 primary ship categories and many non-ship targets based on the Gaofen-3 satellite in scenes such as sea, land, coast, river, and island. Based on the experimental setting of (Wang et al., 2022a), we have ten types of ocean target slices from origin images, such as four fine-grained ships, bridges, and ocean scene slices. We use this dataset to evaluate the fine-grained classification performance for ocene targets.

SAR-ACD (Sun et al., 2022) contains six types of aircraft based on the Gaofen-3 satellite in three civil airports, including Shanghai Hongqiao Airport, Beijing Capital Airport, and Taiwan Taoyuan Airport. Since the released dataset does not separate the training and test data, we randomly select

**Table 2**  
Experimental setting.

Pre-training setting	
Config	Value
optimizer	AdamW
base learning rate	1e-3
weight decay	0.05
optimizer momentum	$\beta_1, \beta_2 = 0.9, 0.95$
batch size	300
epoch	200
learning rate schedule	cosine decay
warmup epoch	20
augmentation	ResizedCrop, HFlip, Contrast
Classification settings	
Config	Value
optimizer	AdamW
base learning rate	1e-3
weight decay	5e-4
optimizer momentum	$\beta_1, \beta_2 = 0.9, 0.999$
batch size	50
epoch	40
learning rate schedule	cosine decay
warmup epoch	2
warmup type	constant
warmup learning rate	1e-5

small samples as the training set and others as the test set. We use this dataset to evaluate fine-grained aircraft target classification. Fine-grained recognition of aircraft targets is a more challenging task due to the smooth surface of the aircraft, resulting in insignificant features.

**Experimental settings.** Table 2 gives the default setting. The pre-training is applied on 4 NVIDIA V100 GPUs with 200 epochs and 300 batch sizes, and the backbone model is ViT-Base (ViT-B). Other specific hyperparameters of each method use the default settings from their papers and codes. Compared to the training settings of MAE, we add ColorJitter (contrast = 0.5) to increase data richness, and all methods use the same data augmentation. Since our goal is not to get better performance by tuning downstream hyperparameters, all models use the same training settings in downstream classification tasks. The few-shot learning setting is based on the Dassel toolbox (Zhou et al., 2023a) and is averaged over 10 random experiments.

## 4.2. Ablation Study

Here, we analyze three key points of the proposed method. The first compares local (LoMaR) and global (MAE) mask methods and explains why we apply LoMaR with its modified ViT and MAE's deep decoder as the backbone. Then, we discuss different target features (LPF, HOG, SAR-HOG, and ours) on the same backbone to show the need for suppressing noise and target features. Finally, we discuss the role of MIM and PGCA in our architecture.

**LoMaR vs. MAE.** Since most targets are small objects in remote sensing images, we prefer masking in local areas to learn the contextual relationships near the target better.

Compared to MAE, which masks over the whole image, LoMaR randomly selects multiple local squares for masking. In addition to this, LoMaR uses relative positional encoding, input with mask tokens, and linear decoder. As LoMaR emphasizes, the first two are indispensable to prevent feature collapse. When we remove any of them, pre-training in SAR images with LoMaR and LoMaR-SAR have performance degradation and feature collapse.

LoMaR uses a linear decoder to speed up the computation. However, the linear layer is unsuitable for SAR images because SAR image noise is easier than a deep decoder to affect the encoder features through the loss function. In our early experiments, LoMaR performed better than MAE on small batches of high-quality pre-training data. When we extended the pre-training set to different quality datasets, LoMaR's performance became unstable. This phenomenon inspired us to make improvements to the decoder and target features. As shown in Table 3, LoMaR-SAR, which replaces the linear decoder of LoMaR with an eight-layer decoder in MAE<sup>4</sup>, has the best result. Therefore, we use LoMaR-SAR as the MIM module for SAR-JEPA. The target encoder for SAR-JEPA is discussed below. It needs unique designs for SAR images and is at the heart of our architecture.

**Target feature selection.** In Table 4, we compare the results of pixel value, Low Pass Filter (LPF) (Liu et al., 2023), SAR-HOG (Song et al., 2016), and Gradient-by-Ratio (GR) (Dellinger et al., 2014). All the changes are made only in the target features, while other settings remain unchanged. The Pixel in Table 4 is LoMaR-SAR as baseline. The LPF can mitigate noise interference, but we observe a slight drop of LPF compared to Pixel on the MSTAR's linear probing result. Therefore, inspired by the HOG feature in MaskFeat, we prefer to obtain high-quality target features with suppressing noise.

Although HOG features have shown effectiveness in FG-MAE for SAR scene-level SSL, we found that the HOG features are unsuitable for target-level SSL in Table 4. This result is because speckle noise can cause the gradient computation in small target regions to have many noise points, greatly affecting the quality of target features. Inspired by the physics-guided contrastive architecture using SAR physics features, we investigate the HOG feature variant in the SAR domain, *i.e.*, SAR-HOG. The core of SAR-HOG is the change in the gradient calculation from differential gradient to ratio gradient. As shown in Table 4, we observe a significant improvement compared to HOG due to this modification. However, the sampling method of HOG may lead to the loss of some small target scattering points, such as the discrete points of an aircraft or a small boat. Therefore, we focus on the gradient information, *i.e.*, target edges. Moreover, basic information, such as the shape and edges of an object, is a generic property (Liu et al., 2022; Cheng et al., 2022; Shi et al., 2020).

<sup>4</sup>However, deeper decoders can be detrimental to encoder performance. For example, the twelve-layer decoder is worse than the eight-layer in the MAE paper.

**Table 3**

Discussion of the MIM framework for SAR-JEPA. MAE performs global masks, and LoMaR performs local masks. LoMaR-SAR is our modified LoMaR with decoder depth, and we use it as our SAR-JEPA backbone. The classification metric is average accuracy (%). **Bold** indicates the best result, underline indicates the next best result.

fine-tuning									
Method	MSTAR			FUSAR-Ship			SAR-ACD		
	10-shot	20-shot	40-shot	10-shot	20-shot	40-shot	10-shot	20-shot	40-shot
MAE (He et al., 2022)	<u>50.6</u>	61.3	69.5	71.7	75.4	78.2	<u>51.6</u>	<u>57.0</u>	<u>69.5</u>
LoMaR (Chen et al., 2022a)	45.6	<u>62.9</u>	<u>77.0</u>	<u>75.9</u>	<u>80.2</u>	<u>82.7</u>	51.2	54.4	67.4
LoMaR-SAR*	<b>55.3</b>	<b>69.8</b>	<b>84.5</b>	<b>78.6</b>	<b>82.0</b>	<b>84.8</b>	<b>51.7</b>	<b>60.1</b>	<b>71.7</b>
linear probing									
Method	MSTAR			FUSAR-Ship			SAR-ACD		
	10-shot	20-shot	40-shot	10-shot	20-shot	40-shot	10-shot	20-shot	40-shot
MAE (He et al., 2022)	<u>53.7</u>	<u>59.2</u>	<u>63.7</u>	<u>74.2</u>	<u>78.1</u>	80.3	<u>49.9</u>	<u>56.9</u>	<u>62.7</u>
LoMaR (Chen et al., 2022a)	39.3	48.9	55.6	70.5	77.9	<u>80.7</u>	47.8	53.4	59.1
LoMaR-SAR*	<b>57.7</b>	<b>64.4</b>	<b>72.2</b>	<b>78.0</b>	<b>81.0</b>	<b>84.0</b>	<b>54.4</b>	<b>58.9</b>	<b>64.4</b>

\* We replace the linear decoder of LoMaR with an eight-layer decoder in MAE to reduce the effect of noise in the reconstructed pixels by increasing the decoder depth. This improvement inspired us to resolve thoroughly SAR image noise with high-quality target features.

**Table 4**

Results of different target features for SAR-JEPA. LPF: low pass filter. HOG: histogram of oriented gradient. GR: gradient-by-ratio. The baseline is pixel value, which is corresponds to LoMaR-SAR in Table 3. LPF uses the default filter hyperparameters in (Liu et al., 2023). SAR-HOG and two GR method, whose kernel size can be adjusted, use the same multi-scale setting. GR<sub>lin</sub>: gradient-by-ratio with linear kernel. GR<sub>Gau</sub>: gradient-by-ratio with Gaussian kernel. The classification metric is average accuracy (%). **Bold** indicates the best result, underline indicates the next best result.

fine-tuning									
Target feature	MSTAR			FUSAR-Ship			SAR-ACD		
	10-shot	20-shot	40-shot	10-shot	20-shot	40-shot	10-shot	20-shot	40-shot
Pixel	55.3	69.8	84.5	78.6	82.0	84.8	51.7	60.1	71.7
LPF (Liu et al., 2023)	57.7	72.7	86.5	78.4	81.9	84.9	51.9	61.2	72.8
HOG (Wei et al., 2022)	30.2	32.4	40.3	58.1	63.3	66.6	51.7	57.9	64.7
SAR-HOG (Song et al., 2016)	<u>64.4</u>	76.4	<u>90.5</u>	76.7	80.8	85.3	51.4	60.0	73.4
GR <sub>Gau</sub> * (Dellinger et al., 2014)	<u>62.8</u>	<u>78.5</u>	<u>88.2</u>	<u>80.6</u>	<u>82.8</u>	<b>86.0</b>	<b>55.3</b>	<b>62.9</b>	<u>73.0</u>
GR <sub>lin</sub> (Song et al., 2016)	<b>70.3</b>	<b>82.1</b>	<b>91.6</b>	<b>81.3</b>	<b>83.3</b>	<u>85.8</u>	<u>54.8</u>	<u>62.6</u>	<b>75.5</b>
linear probing									
Target feature	MSTAR			FUSAR-Ship			SAR-ACD		
	10-shot	20-shot	40-shot	10-shot	20-shot	40-shot	10-shot	20-shot	40-shot
Pixel	57.7	64.4	72.2	78.0	81.0	84.0	54.4	58.9	64.4
LPF (Liu et al., 2023)	56.1	62.6	68.1	78.7	82.0	84.6	54.9	59.5	65.2
HOG (Wei et al., 2022)	33.3	37.8	41.6	52.6	58.3	61.5	49.2	53.1	56.7
SAR-HOG (Song et al., 2016)	58.9	68.1	77.1	79.3	81.8	85.0	54.6	59.3	66.5
GR <sub>Gau</sub> * (Dellinger et al., 2014)	<u>62.8</u>	<u>72.3</u>	<u>77.6</u>	<b>82.0</b>	<b>82.9</b>	<b>85.7</b>	<u>54.7</u>	<b>60.9</b>	<u>66.6</u>
GR <sub>lin</sub> (Song et al., 2016)	<b>67.7</b>	<b>75.1</b>	<b>81.6</b>	<u>80.6</u>	<u>82.7</u>	<u>85.2</u>	<b>56.8</b>	<u>60.4</u>	<b>66.8</b>

\* We finally chose the linear kernel GR<sub>lin</sub> for SAR-JEPA because it needed a lot of time to fine-tune the Gaussian kernel GR<sub>Gau</sub> parameters in pre-training. And we set the Gaussian standard deviation from  $\sigma = 0.3 * ((2r + 1 - 1) * 0.5 - 1) + 0.8$ . It means the standard deviation is related to the kernel size instead of a fixed parameter in Dellinger et al. (2014).

We consider two versions of GR in SAR. GR<sub>lin</sub> is computing gradient with a linear kernel (Song et al., 2016) whose  $M$  value equals 1. GR<sub>Gau</sub> is computing gradient with a Gaussian kernel (Dellinger et al., 2014) whose  $M$  value obeys a Gaussian distribution. Table 4 shows that the two calculation methods have their advantages for different target categories and have similar performance in most cases. The

Gaussian kernel can act as a filter, but the parameters need to be adjusted so as not to blur the target edges overly. Because a pre-trained model needs tens of hours to several days, we prefer to use simple and effective methods with scaling data and parameters. Therefore, we use a linear kernel without spending too much time tuning the parameters of the Gaussian kernel at different scales.

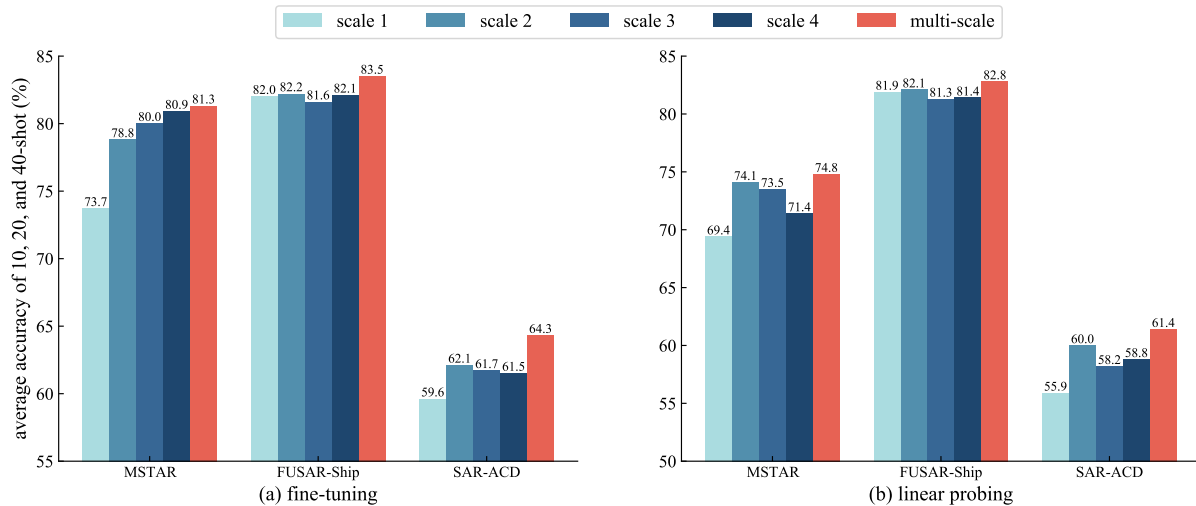


**Figure 4:** Multi-scale kernel settings for gradient-by-ratio  $GR_{lin}$ . Here, the scale 1/2/3/4 is with  $r$  equal to 5/7/13/17, and the multi-scale concat all four scales in feature channel. Multi-scale is more suitable than single scale due to various targets in remote sensing images.

**Table 5**

Ablation study of our SAR-JEPA, which is a combination of two architectures (MIM and PGCA). The classification metric is average accuracy (%). **Bold** indicates the best result, underline indicates the next best result.

fine-tuning									
Method	MSTAR			FUSAR-Ship			SAR-ACD		
	10-shot	20-shot	40-shot	10-shot	20-shot	40-shot	10-shot	20-shot	40-shot
MIM*	55.3	69.8	84.5	<u>78.6</u>	<u>82.0</u>	<u>84.8</u>	51.7	<u>60.1</u>	71.7
PGCA**	<u>56.7</u>	<u>71.4</u>	<u>88.1</u>	76.4	80.4	83.8	<u>51.8</u>	60.0	<u>73.7</u>
SAR-JEPA	<b>70.3</b>	<b>82.1</b>	<b>91.6</b>	<b>81.3</b>	<b>83.3</b>	<b>85.8</b>	<b>54.8</b>	<b>62.6</b>	<b>75.5</b>
linear probing									
Method	MSTAR			FUSAR-Ship			SAR-ACD		
	10-shot	20-shot	40-shot	10-shot	20-shot	40-shot	10-shot	20-shot	40-shot
MIM*	57.7	64.4	72.2	<u>78.0</u>	81.0	84.0	54.4	58.9	64.4
PGCA**	<u>61.0</u>	<u>68.0</u>	<u>74.7</u>	77.4	<u>81.6</u>	<u>84.2</u>	52.7	58.3	<u>66.1</u>
SAR-JEPA	<b>67.7</b>	<b>75.1</b>	<b>81.6</b>	<b>80.6</b>	<b>82.7</b>	<b>85.2</b>	<b>56.8</b>	<b>60.4</b>	<b>66.8</b>

\* MIM is refers to LoMaR-SAR in Table 3, which is also the MIM module of our SAR-JEPA.

\*\* Due to PGCA (Datcu et al., 2023) using complex SAR image's features as target signal, we follow its ideas and use our target encoder. Here, PGCA is the contrastive learning between deep features and our multi-scale gradient features  $GR_{lin}$  to test the effectiveness of the target feature as a guided signal, *w.r.t.*, it removes the MIM task in SAR-JEPA.

Another important thing is that we propose a multi-scale setting instead of single-scale features for various targets included in the pre-training set. Multi-scale can improve the feature representation for various targets in remote sensing. Figure 4 gives the result of different kernel settings. Scale settings have various effects: smaller scales can better extract small target edges, while larger scales are more obvious for noise suppression. Hence, learning target features at different scales is more advantageous than a single scale.

**SAR-JEPA** is a combination of MIM and PGCA ideas as shown in Figure 1. Specifically, we designed LoMaR-SAR and multi-scale gradient features as a concrete implementation of the MIM and target encoder module. Table 5 demonstrates the equal importance and mutual reinforcement of

the two modules. These focus on the pretext task and signal quality of SSL driven by the data. MIM can provide PGCA with a challenging pretext task of learning features with contextual information in the image. PGCA can improve the quality of features by introducing domain knowledge into the embedding of the target encoder. Combining MIM and PGCA, SAR-JEPA learns high-quality contextual features for low-quality noisy SAR data.

### 4.3. Comparisons with other methods

As shown in Table 6, we evaluated the SSL methods in few-shot classification tasks. The comparison methods are ImageNet, MAE (He et al., 2022), Feature Guided MAE (FG-MAE) (Wang et al., 2023d), I-JEPA (Assran et al.,

**Table 6**

 Fine-grained classification results of different methods. The classification metric is average accuracy (%). **Bold** indicates the best result, underline indicates the next best result.

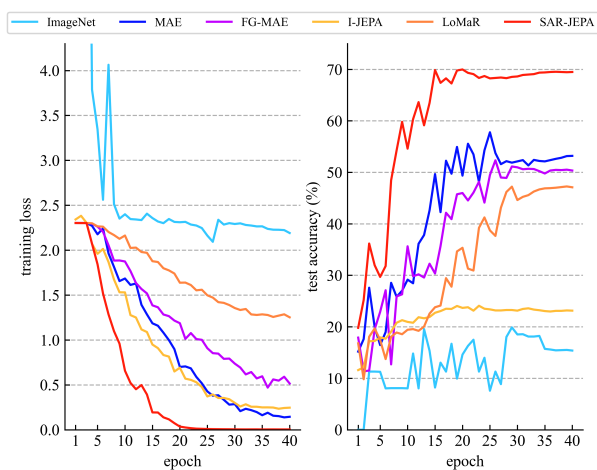
MSTAR								
Method	Mask area	Target feature	fine-tuning			linear probing		
			10-shot	20-shot	40-shot	10-shot	20-shot	40-shot
ImageNet	-	-	16.7	32.0	40.7	45.0	56.3	<u>66.8</u>
MAE (He et al., 2022)	Global	Pixel value	<u>50.6</u>	61.3	69.5	<u>53.7</u>	<u>59.2</u>	63.7
FG-MAE (Wang et al., 2023d)	Global	HOG	50.0	58.7	70.0	43.5	50.7	56.4
I-JEPA (Assran et al., 2023)	Global	Deep feature	24.5	33.4	44.6	30.9	38.6	44.7
LoMaR (Chen et al., 2022a)	Local	Pixel value	45.6	<u>62.9</u>	<u>77.0</u>	39.3	48.9	55.6
<b>SAR-JEPA</b>	Local	GR <sub>lin</sub>	<b>70.3</b>	<b>82.1</b>	<b>91.6</b>	<b>67.7</b>	<b>75.1</b>	<b>81.6</b>

FUSAR-ship								
Method	Mask area	Target feature	fine-tuning			linear probing		
			10-shot	20-shot	40-shot	10-shot	20-shot	40-shot
ImageNet	-	-	54.0	57.0	59.7	<u>74.6</u>	<u>79.6</u>	<u>83.6</u>
MAE (He et al., 2022)	Global	Pixel value	71.7	75.4	78.2	74.2	78.1	80.3
FG-MAE (Wang et al., 2023d)	Global	HOG	65.5	73.7	76.6	69.7	74.3	77.7
I-JEPA (Assran et al., 2023)	Global	Deep feature	38.5	38.9	49.4	36.5	42.2	46.8
LoMaR (Chen et al., 2022a)	Local	Pixel value	<u>75.9</u>	<u>80.2</u>	<u>82.7</u>	70.5	77.9	80.7
<b>SAR-JEPA</b>	Local	GR <sub>lin</sub>	<b>81.3</b>	<b>83.3</b>	<b>85.8</b>	<b>80.6</b>	<b>82.7</b>	<b>85.2</b>

SAR-ACD								
Method	Mask area	Target feature	fine-tuning			linear probing		
			10-shot	20-shot	40-shot	10-shot	20-shot	40-shot
ImageNet	-	-	22.6	26.8	42.7	34.8	44.2	54.2
MAE (He et al., 2022)	Global	Pixel value	<u>51.6</u>	<u>57.0</u>	<u>69.5</u>	<u>49.9</u>	<u>56.9</u>	<u>62.7</u>
FG-MAE (Wang et al., 2023d)	Global	HOG	50.4	54.2	62.9	47.5	51.5	57.0
I-JEPA (Assran et al., 2023)	Global	Deep feature	45.0	51.7	63.3	42.7	51.0	60.0
LoMaR (Chen et al., 2022a)	Local	Pixel value	51.2	54.4	67.4	47.8	53.4	59.1
<b>SAR-JEPA</b>	Local	GR <sub>lin</sub>	<b>54.8</b>	<b>62.6</b>	<b>75.5</b>	<b>56.8</b>	<b>60.4</b>	<b>66.8</b>



**Figure 5:** Training loss and test accuracy curves for one fine-tuning of MSTAR 10-shot in Table 6. From the figure, effective self-supervised learning decreases the training loss rapidly and converges to a better-generalized region.

2023), LoMaR (Chen et al., 2022a), and Our SAR-JEPA. Table 6 also gives the difference in the mask area and target

features. The ImageNet migrated the supervised pre-training weights on the ImageNet as initialization.

Table 6 studies the result of different pre-trained models on fine-grained SAR target classification. Due to the large difference between SAR and RGB images, ImageNet weights are hard to obtain effective features with small samples under fine-tuning, and using linear probing can have a better result with an unsuitable initialization weight. MAE trained on the SAR dataset performs better than ImageNet with fine-tuning, but the speckle noise affects its representation quality. HOG is not an effective solution to the speckle noise because multiplicative noise leads to the virtual dots in the strong scattering region. It results in a performance degradation in FG-MAE with HOG features, and FG-MAE converges slower than MAE in Figure 5. Our method is a special form of the I-JEPA (Assran et al., 2023) method in SAR. But I-JEPA has the feature collapse, in which the learnable predictor fails to learn a good feature space under speckle noise. In Figure 5, I-JEPA converges to a region with poor test performance. Figure 5 also shows that effective self-supervised learning decreases the training loss rapidly and converges to a better-generalized region

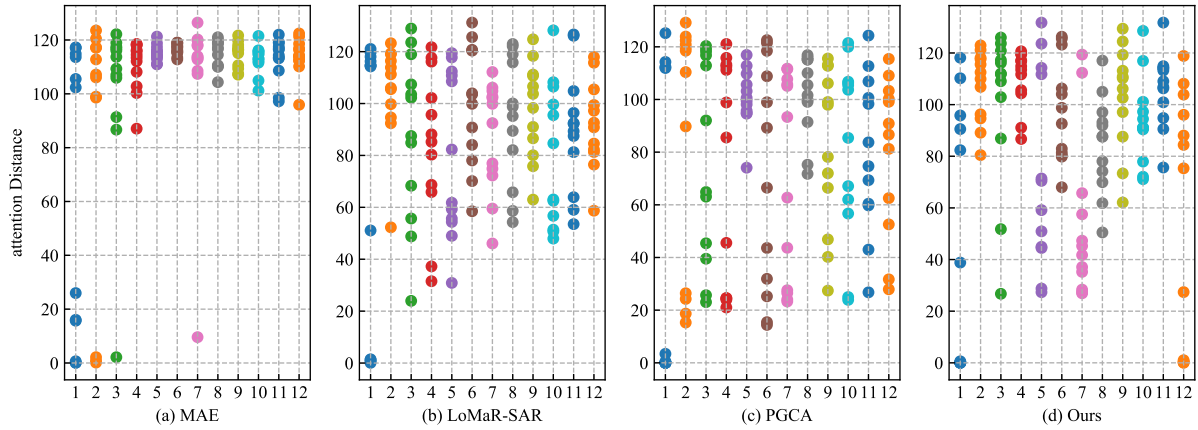


**Figure 6:** The averaged attention distance of ViT with different methods. The X-axis is the attention head *i.e.* layer number. MAE focuses on global information, and other methods have local and global attention ranges. It shows that using pixel-level features as a pretext task with a local image scale can enhance the diversity of Vit modeling with SAR images.

Another interesting phenomenon is the range of contexts, where it can be found that LoMaR with local reconstruction can achieve better fine-tuning results in vehicle and ship compared to MAE. This result illustrates the need to consider the range of contextual information in remote-sensing images. However, due to a linear decoder, LoMaR is more susceptible to the effects of speckle noise in the pixels, leading to unstable performance in Table 6 and slow convergence rate in Figure 5.

Although the proposed method achieves better results on the aircraft dataset, it is not as good as vehicle and ship results. In particular, fine-tuning at SAR-ACD 10-shot is worse than the linear probing, indicating slight overfitting phenomena. It is because the aircraft reflects electromagnetic waves with its streamlined structure, resulting in SAR images that may lack the complete aircraft structure, with only some strong scattering points and shadow edges. Besides, our pre-training did not include many aircraft target samples. Because of this, the generic representation in SAR images still needs to be further explored.

#### 4.4. Visualization

Compared to supervised pre-training and contrastive learning, which have a local attention range in the high layer, ViT with MIM has various attention ranges in different layers (Xie et al., 2023b). However, Figure 6 shows that this characteristic of MIM is related to data property and pixel-level pretext task. We first notice that the deep layers of MAE mainly focus on global information due to large SAR image scenes, which differs from MIM’s modeling properties with ImageNet. Then, LoMaR-SAR with local reconstruction acquires the ability to model local information. This phenomenon illustrates that local information is easily lost in remote sensing images, and local reconstruction can better capture contextual details. In addition, PGCA, which removes the mask in SAR-JEPA and has a pixel-level contrast learning task, can acquire local information. It

suggests that the property of modeling local and global information originates from the pixel-level pretext task. Finally, our SAR-JEPA with integrated MIM and PGCA can model local and global features. It can be found that the addition of MIM makes SAR-JEPA pay more attention to high-level global contextual information and more diminished attention to local edge features compared to PGCA. Therefore, the differences in the properties between SAR and RGB images make the same self-supervised learning method show different properties, which is a great challenge for the SSL methods in SAR.

#### 4.5. Scaling Experiment

MIM can benefit from scaling data, model parameters, and computational resources, but it will suffer from overfitting when using small data and long training epochs on large models (Xie et al., 2023c). Therefore, we evaluate the scalability of SAR-JEPA with linear probing performance on SAR data. Figure 7 gives the scaling experiment in dataset size, model parameters, and training epoch.

**Dataset size.** A significant performance increase is observed in small-sample classification with increasing data volume. This phenomenon suggests that by extracting high-quality features as guide signals, self-supervised learning performance can be improved by increasing the number of noisy SAR images. Moreover, this result indicates that SSL does not reach saturation in dataset size and has a huge potential for foundation model to be exploited.

**Model parameters.** As the model parameters increase, we also observe an increase in representation quality. However, ViT-Large suffered from overfitting problems due to insufficient dataset size and has reduced performance in the fine-grained classification of vehicles and aircraft.

**Training epoch.** Similarly, too-long training epochs result in the overfitting of ViT-Base, and thereby, our default training setting is 200 epochs. Therefore, the next step is to collect more SAR target data to exploit the potential of SSL and foundation models.

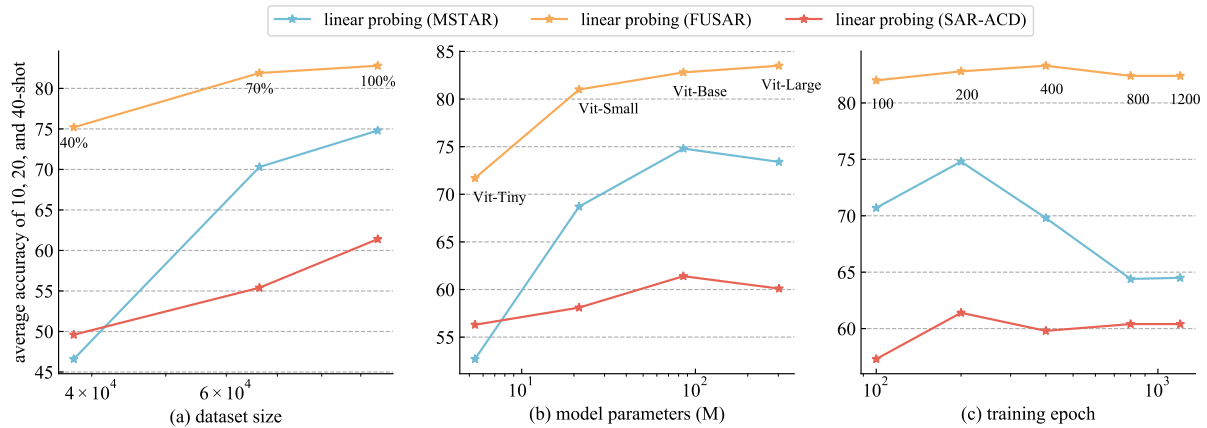


**Figure 7:** Scaling experiment of SAR-JEPA in dataset size, model parameters, and training epoch. We find that SAR-JEPA can benefit from these three aspects, but due to the limitation of dataset size, a large model and long training epochs lead to overfitting and reduce the linear probing performance.

## 5. Conclusion

In our work, we investigate the SSL for SAR ATR with our SAR-JEPA. SAR-JEPA combines two architectures to perform mask image modeling in gradient feature space for SAR images. By leveraging SAR domain features, we extend the applicability of MIM to SAR imagery, a type of noisy remote sensing data. Through extensive experimentation and analysis, we demonstrate the effectiveness of the proposed SAR-JEPA in obtaining high-quality representations for SAR ATR. Our research highlights the importance of embracing SSL to take advantage of the increasing availability of SAR data. The large pre-training samples. In the future, we will further extend the data and computational resources. give SSL the potential to achieve a foundation model for various downstream SAR ATR tasks across targets, scenes, and sensors.

However, it is worth noting that our pre-training dataset<sup>5</sup> is not as extensive as ImageNet to fully exploit the potential of SSL for SAR ATR. In addition, it needs further investigation for other foundation model architectures, such as ConvNeXt. While our work primarily focuses on feature representation across different targets, it is essential to explore and discuss various tasks, including detection and segmentation. In the future, we plan to enhance our proposed scheme by improving data collection methods, refining model architectures, and exploring novel pre-training target features. Our ultimate goal is to successfully apply the foundation model with SSL in SAR target recognition.

## References

Air Force Research Laboratory, . The air force moving and stationary

<sup>5</sup>To the best of our knowledge, other SAR datasets can be further added to the pre-training, such as vehicle (Gotcha (Dungan et al., 2012), SIVED (Lin et al., 2023)), ship datasets (AIR-SARSHIP Sun et al. (2019), HRSID (Wei et al., 2020)), aircraft dataset (SADD Zhang et al. (2022)), and building datasets (FUSAR-Map Shi et al. (2021), OGSOD (Wang et al., 2023a)). However, how to further scale the SAR target data volume close to the million scale of ImageNet is a challenging problem.

target recognition database. <https://www.sdms.afrl.af.mil/index.php?collection=mstar>.

- Assran, M., Duval, Q., Misra, I., Bojanowski, P., Vincent, P., Rabat, M., LeCun, Y., Ballas, N., 2023. Self-supervised learning from images with a joint-embedding predictive architecture, in: Proc. IEEE Comput. Soc. Conf. Comput. Vis. Pattern Recognit. (CVPR), pp. 15619–15629.
- Balestriero, R., Ibrahim, M., Sobal, V., Morcos, A., Shekhar, S., Goldstein, T., Bordes, F., Bardes, A., Mialon, G., Tian, Y., et al., 2023. A cookbook of self-supervised learning. arXiv preprint URL: <https://arxiv.org/abs/2304.12210>.
- Bao, H., Dong, L., Piao, S., Wei, F., 2021. BEiT: BERT pre-training of image transformers, in: Proc. Int. Conf. Learn. Represent. (ICLR).
- Bovik, A.C., 1986. On detecting edges in speckle imagery. IEEE Trans. Acoust. Speech Signal Process. 36, 1618–1627.
- Canny, J., 1986. A computational approach to edge detection. IEEE Trans. Pattern Anal. Mach. Intell. , 679–698.
- Chen, J., Hu, M., Li, B., Elhoseiny, M., 2022a. Efficient self-supervised vision pretraining with local masked reconstruction. arXiv preprint URL: <https://arxiv.org/abs/2206.00790>.
- Chen, J., Huang, Z., Xia, R., Wu, B., Sheng, L., Sun, L., Yao, B., 2022b. Large-scale multi-class SAR image target detection dataset-1.0. <https://radars.ac.cn/web/data/getData?dataType=MSAR>.
- Chen, Y., Bruzzone, L., 2022. Self-supervised SAR-optical data fusion of Sentinel-1/-2 images. IEEE Trans. Geosci. Remote Sens. 60, 1–11. doi:10.1109/TGRS.2021.3128072.
- Cheng, G., Yuan, X., Yao, X., Yan, K., Zeng, Q., Xie, X., Han, J., 2023. Towards large-scale small object detection: Survey and benchmarks. IEEE Trans. Pattern Anal. Mach. Intell. 45, 13467–13488. doi:10.1109/TPAMI.2023.3290594.
- Cheng, M.M., Gao, S.H., Borji, A., Tan, Y.Q., Lin, Z., Wang, M., 2022. A highly efficient model to study the semantics of salient object detection. IEEE Trans. Pattern Anal. Mach. Intell. 44, 8006–8021. doi:10.1109/TPAMI.2021.3107956.
- Datcu, M., Huang, Z., Anghel, A., Zhao, J., Cacoveanu, R., 2023. Explainable, physics-aware, trustworthy artificial intelligence: A paradigm shift for synthetic aperture radar. IEEE Geosci. Remote Sens. Mag. 11, 8–25.
- Dellinger, F., Delon, J., Gousseau, Y., Michel, J., Tupin, F., 2014. SAR-SIFT: a SIFT-like algorithm for SAR images. IEEE Trans. Geosci. Remote Sens. 53, 453–466.
- Dong, G., Liu, H., Chanussot, J., 2020. Keypoint-based local descriptors for target recognition in SAR images: A comparative analysis. IEEE Geosci. Remote Sens. Mag. 9, 139–166.
- Dosovitskiy, A., Beyer, L., Kolesnikov, A., Weissenborn, D., Zhai, X., Unterthiner, T., Dehghani, M., Minderer, M., Heigold, G., Gelly, S., et al., 2020. An image is worth 16x16 words: Transformers for image recognition at scale. arXiv preprint URL: <https://arxiv.org/abs/2010>.

- 11929.
- Dungan, K.E., Ash, J.N., Nehrbass, J.W., Parker, J.T., Gorham, L.A., Scarborough, S.M., 2012. Wide angle SAR data for target discrimination research, in: Proc. SPIE Conf. Algorithms SAR Imagery, pp. 181–193.
- Fei-Fei, L., Krishna, R., 2022. Searching for computer vision north stars. *Daedalus* 151, 85–99.
- Gagliardi, V., Tosti, F., Bianchini Ciampoli, L., Battagliere, M.L., D'Amato, L., Alani, A.M., Benedetto, A., 2023. Satellite remote sensing and non-destructive testing methods for transport infrastructure monitoring: Advances, challenges and perspectives. *Remote Sens.* 15, 418.
- Goldblum, M., Souril, H., Ni, R., Shu, M., Prabhu, V.U., Somepalli, G., Chattopadhyay, P., Ibrahim, M., Bardes, A., Hoffman, J., Chellappa, R., Wilson, A.G., Goldstein, T., 2023. Battle of the backbones: A large-scale comparison of pretrained models across computer vision tasks, in: Proc. Adv. Neural Inf. Process. Syst. (NeurIPS). URL: <https://openreview.net/forum?id=1yOnfDpkVe>.
- He, K., Chen, X., Xie, S., Li, Y., Dollár, P., Girshick, R., 2022. Masked autoencoders are scalable vision learners, in: Proc. IEEE Comput. Soc. Conf. Comput. Vis. Pattern Recognit. (CVPR), pp. 16000–16009.
- Hou, X., Ao, W., Song, Q., Lai, J., Wang, H., Xu, F., 2020. FUSAR-Ship: Building a high-resolution SAR-AIS matchup dataset of Gaofen-3 for ship detection and recognition. *Sci. China Inf. Sci.* 63, 1–19.
- Huang, L., Liu, B., Li, B., Guo, W., Yu, W., Zhang, Z., Yu, W., 2017. OpenSARShip: A dataset dedicated to Sentinel-1 ship interpretation. *IEEE J. Sel. Top. Appl. Earth Obs. Remote Sens.* 11, 195–208.
- Huang, Z., Yao, X., Liu, Y., Dumitru, C.O., Datcu, M., Han, J., 2022. Physically explainable CNN for SAR image classification. *ISPRS J. Photogramm. Remote Sens.* 190, 25–37.
- Ibanez, D., Fernandez-Beltran, R., Pla, F., Yokoya, N., 2022. Masked auto-encoding spectral–spatial transformer for hyperspectral image classification. *IEEE Trans. Geosci. Remote Sens.* 60, 1–14.
- Kechagias-Stamatis, O., Aouf, N., 2021. Automatic target recognition on synthetic aperture radar imagery: A survey. *IEEE Aerosp. Electron. Syst. Mag.* 36, 56–81. doi:10.1109/MAES.2021.3049857.
- Kusk, A., Abulaitijiang, A., Dall, J., 2016. Synthetic SAR image generation using sensor, terrain and target models, in: Proc. Eur. Conf. Synth. Aperture Radar, EUSAR 2016, VDE. pp. 1–5.
- Lewis, B., Scarnati, T., Sudkamp, E., Nehrbass, J., Rosencrantz, S., Zelnio, E., 2019. A SAR dataset for ATR development: the synthetic and measured paired labeled experiment (SAMPLE), in: Proc. SPIE Conf. Algorithms SAR Imagery, pp. 39–54.
- Li, J., Yu, Z., Yu, L., Cheng, P., Chen, J., Chi, C., 2023a. A comprehensive survey on SAR ATR in deep-learning era. *Remote Sens.* 15, 1454.
- Li, W., Yang, W., Zhang, W., Liu, T., Liu, Y., Liu, L., 2023b. Hierarchical disentanglement-alignment network for robust SAR vehicle recognition. *IEEE J. Sel. Top. Appl. Earth Obs. Remote Sens.* 16, 9661–9679. doi:10.1109/JSTARS.2023.3324182.
- Li, Y., Hou, Q., Zheng, Z., Cheng, M.M., Yang, J., Li, X., 2023c. Large selective kernel network for remote sensing object detection, in: Proc. IEEE Int. Conf. Comput. Vis. (ICCV), pp. 16794–16805.
- Lin, X., Zhang, B., Wu, F., Wang, C., Yang, Y., Chen, H., 2023. SIVED: A SAR image dataset for vehicle detection based on rotatable bounding box. *Remote Sens.* 15, 2825.
- Liu, X., Zhang, F., Hou, Z., Mian, L., Wang, Z., Zhang, J., Tang, J., 2021. Self-supervised learning: Generative or contrastive. *IEEE Trans. Knowl. Data Eng.* 35, 857–876.
- Liu, Y., Wu, Y.H., Wen, P., Shi, Y., Qiu, Y., Cheng, M.M., 2022. Leveraging instance-, image- and dataset-level information for weakly supervised instance segmentation. *IEEE Trans. Pattern Anal. Mach. Intell.* 44, 1415–1428. doi:10.1109/TPAMI.2020.3023152.
- Liu, Y., Zhang, S., Chen, J., Chen, K., Lin, D., 2023. PixMIM: Rethinking pixel reconstruction in masked image modeling. arXiv preprint URL: <https://arxiv.org/abs/2303.02416>.
- Malmgren-Hansen, D., Kusk, A., Dall, J., Nielsen, A.A., Engholm, R., Skriver, H., 2017. Improving SAR automatic target recognition models with transfer learning from simulated data. *IEEE Geosci. Remote Sens. Lett.* 14, 1484–1488.
- Moreira, A., Prats-Iraola, P., Younis, M., Krieger, G., Hajnsek, I., Papathanassiou, K.P., 2013. A tutorial on synthetic aperture radar. *IEEE Geosci. Remote Sens. Mag.* 1, 6–43. doi:10.1109/MGRS.2013.2248301.
- Pei, H., Su, M., Xu, G., Xing, M., Hong, W., 2023. Self-supervised feature representation for SAR image target classification using contrastive learning. *IEEE J. Sel. Top. Appl. Earth Obs. Remote Sens.* 16, 9246–9258. doi:10.1109/JSTARS.2023.3321769.
- Peng, B., Peng, B., Zhou, J., Xie, J., Liu, L., 2022. Scattering model guided adversarial examples for SAR target recognition: Attack and defense. *IEEE Trans. Geosci. Remote Sens.* 60, 1–17.
- Reed, C.J., Gupta, R., Li, S., Brockman, S., Funk, C., Clipp, B., Keutzer, K., Candido, S., Uyttendaele, M., Darrell, T., 2023. Scale-MAE: A scale-aware masked autoencoder for multiscale geospatial representation learning, in: Proc. IEEE Int. Conf. Comput. Vis. (ICCV), pp. 4088–4099.
- Rizzi, M., Tagliaferri, D., Tebaldini, S., Nicoli, M., Russo, I., Mazzucco, C., Monti-Guarnieri, A.V., Prati, C.M., Spagnolini, U., 2021. Navigation-aided automotive SAR imaging in urban environments, in: Proc. Int. Geosci. Remote. Sens. Symp. (IGARSS), IEEE. pp. 2979–2982.
- Ross, T.D., Bradley, J.J., Hudson, L.J., O'connor, M.P., 1999. SAR ATR: So what's the problem? An MSTAR perspective, in: Proc. SPIE Conf. Algorithms SAR Imagery, pp. 662–672.
- Shi, B., Zhang, D., Dai, Q., Zhu, Z., Mu, Y., Wang, J., 2020. Informative dropout for robust representation learning: A shape-bias perspective, in: Int. Conf. Machin. Learn. (ICML).
- Shi, X., Fu, S., Chen, J., Wang, F., Xu, F., 2021. Object-level semantic segmentation on the high-resolution Gaofen-3 FUSAR-Map dataset. *IEEE J. Sel. Top. Appl. Earth Obs. Remote Sens.* 14, 3107–3119.
- Song, S., Xu, B., Yang, J., 2016. SAR target recognition via supervised discriminative dictionary learning and sparse representation of the SAR-HOG feature. *Remote Sens.* 8, 683.
- Sumbul, G., De Wall, A., Kreuziger, T., Marcelino, F., Costa, H., Benevides, P., Caetano, M., Demir, B., Markl, V., 2021. BigEarthNet-MM: A large-scale, multimodal, multilabel benchmark archive for remote sensing image classification and retrieval [software and data sets]. *IEEE Geosci. Remote Sens. Mag.* 9, 174–180.
- Sun, G.C., Liu, Y., Xiang, J., Liu, W., Xing, M., Chen, J., 2021. Spaceborne synthetic aperture radar imaging algorithms: An overview. *IEEE Geosci. Remote Sens. Mag.* 10, 161–184.
- Sun, X., Lv, Y., Wang, Z., Fu, K., 2022. SCAN: Scattering characteristics analysis network for few-shot aircraft classification in high-resolution SAR images. *IEEE Trans. Geosci. Remote Sens.* 60, 1–17. doi:10.1109/TGRS.2022.3166174.
- Sun, X., Wang, P., Lu, W., Zhu, Z., Lu, X., He, Q., Li, J., Rong, X., Yang, Z., Chang, H., He, Q., Yang, G., Wang, R., Lu, J., Fu, K., 2023. RingMo: A remote sensing foundation model with masked image modeling. *IEEE Trans. Geosci. Remote Sens.* 61, 1–22. doi:10.1109/TGRS.2022.3194732.
- Sun, X., Wang, Z., Sun, Y., Diao, W., Zhang, Y., Fu, K., 2019. AIR-SARShip-1.0: High-resolution SAR ship detection dataset. *J. Radars* 8, 852–862. doi:10.12000/JR19097.
- Tao, C., Qi, J., Zhang, G., Zhu, Q., Lu, W., Li, H., 2023. TOV: The original vision model for optical remote sensing image understanding via self-supervised learning. *IEEE J. Sel. Top. Appl. Earth Obs. Remote Sens.* 16, 4916–4930. doi:10.1109/JSTARS.2023.3271312.
- Touzi, R., Lopes, A., Bousquet, P., 1988. A statistical and geometrical edge detector for SAR images. *IEEE Trans. Geosci. Remote Sens.* 26, 764–773.
- Tsokas, A., Rysz, M., Pardalos, P.M., Dipple, K., 2022. SAR data applications in earth observation: An overview. *Expert Syst. Appl.* 205, 117342.
- Wang, C., Ruan, R., Zhao, Z., Li, C., Tang, J., 2023a. Category-oriented localization distillation for SAR object detection and a unified benchmark. *IEEE Trans. Geosci. Remote Sens.* 61, 1–14. doi:10.1109/TGRS.2023.3291356.
- Wang, D., Song, Y., Huang, J., An, D., Chen, L., 2022a. SAR target classification based on multiscale attention super-class network. *IEEE J. Sel. Top. Appl. Earth Obs. Remote Sens.* 15, 9004–9019.
- Wang, H., Song, K., Fan, J., Wang, Y., Xie, J., Zhang, Z., 2023b. Hard patches mining for masked image modeling, in: Proc. IEEE Comput.

- Soc. Conf. Comput. Vis. Pattern Recognit. (CVPR), pp. 10375–10385.
- Wang, H., Tang, Y., Wang, Y., Guo, J., Deng, Z.H., Han, K., 2023c. Masked image modeling with local multi-scale reconstruction, in: Proc. IEEE Comput. Soc. Conf. Comput. Vis. Pattern Recognit. (CVPR), pp. 2122–2131.
- Wang, K., Zhang, G., Leung, H., 2019. SAR target recognition based on cross-domain and cross-task transfer learning. *IEEE Access* 7, 153391–153399.
- Wang, Y., Albrecht, C.M., Braham, N.A.A., Mou, L., Zhu, X.X., 2022b. Self-supervised learning in remote sensing: A review. *IEEE Geosci. Remote Sens. Mag.* 10, 213–247. doi:10.1109/MGRS.2022.3198244.
- Wang, Y., Hernández, H.H., Albrecht, C.M., Zhu, X.X., 2023d. Feature guided masked autoencoder for self-supervised learning in remote sensing. arXiv preprint URL: <https://arxiv.org/abs/2310.18653>.
- Wei, C., Fan, H., Xie, S., Wu, C.Y., Yuille, A., Feichtenhofer, C., 2022. Masked feature prediction for self-supervised visual pre-training, in: Proc. IEEE Comput. Soc. Conf. Comput. Vis. Pattern Recognit. (CVPR), pp. 14668–14678.
- Wei, S., Zeng, X., Qu, Q., Wang, M., Su, H., Shi, J., 2020. HRSID: A high-resolution SAR images dataset for ship detection and instance segmentation. *Ieee Access* 8, 120234–120254.
- Wen, Z., Liu, Z., Zhang, S., Pan, Q., 2021. Rotation awareness based self-supervised learning for SAR target recognition with limited training samples. *IEEE Trans. Image Process.* 30, 7266–7279.
- Wu, K., Peng, H., Chen, M., Fu, J., Chao, H., 2021. Rethinking and improving relative position encoding for vision transformer, in: Proc. IEEE Comput. Soc. Conf. Comput. Vis. Pattern Recognit. (CVPR), pp. 10033–10041.
- Xia, R., Chen, J., Huang, Z., Wan, H., Wu, B., Sun, L., Yao, B., Xiang, H., Xing, M., 2022. CRTransSAR: A visual transformer based on contextual joint representation learning for SAR ship detection. *Remote Sens.* 14, 1488.
- Xie, J., Li, W., Zhan, X., Liu, Z., Ong, Y.S., Loy, C.C., 2023a. Masked frequency modeling for self-supervised visual pre-training, in: Proc. Int. Conf. Learn. Represent. (ICLR).
- Xie, Z., Geng, Z., Hu, J., Zhang, Z., Hu, H., Cao, Y., 2023b. Revealing the dark secrets of masked image modeling, in: Proc. IEEE Comput. Soc. Conf. Comput. Vis. Pattern Recognit. (CVPR), pp. 14475–14485.
- Xie, Z., Zhang, Z., Cao, Y., Lin, Y., Bao, J., Yao, Z., Dai, Q., Hu, H., 2022. SimMIM: A simple framework for masked image modeling, in: Proc. IEEE Comput. Soc. Conf. Comput. Vis. Pattern Recognit. (CVPR), pp. 9653–9663.
- Xie, Z., Zhang, Z., Cao, Y., Lin, Y., Wei, Y., Dai, Q., Hu, H., 2023c. On data scaling in masked image modeling, in: Proc. IEEE Comput. Soc. Conf. Comput. Vis. Pattern Recognit. (CVPR), pp. 10365–10374.
- Zhai, Y., Zhou, W., Sun, B., Li, J., Ke, Q., Ying, Z., Gan, J., Mai, C., Labati, R.D., Piuri, V., Scotti, F., 2022. Weakly contrastive learning via batch instance discrimination and feature clustering for small sample SAR ATR. *IEEE Trans. Geosci. Remote Sens.* 60, 1–17. doi:10.1109/TGRS.2021.3066195.
- Zhang, P., Xu, H., Tian, T., Gao, P., Li, L., Zhao, T., Zhang, N., Tian, J., 2022. SEFEPNet: Scale expansion and feature enhancement pyramid network for SAR aircraft detection with small sample dataset. *IEEE J. Sel. Top. Appl. Earth Obs. Remote Sens.* 15, 3365–3375. doi:10.1109/JSTARS.2022.3169339.
- Zhao, Y., Zhao, L., Liu, Z., Hu, D., Kuang, G., Liu, L., 2022. Attentional feature refinement and alignment network for aircraft detection in SAR imagery. *IEEE Trans. Geosci. Remote Sens.* 60, 1–16. doi:10.1109/TGRS.2021.3139994.
- Zhou, K., Liu, Z., Qiao, Y., Xiang, T., Loy, C.C., 2023a. Domain generalization: A survey. *IEEE Trans. Pattern Anal. Mach. Intell.* 45, 4396–4415.
- Zhou, Y., Chia, M.A., Wagner, S.K., Ayhan, M.S., Williamson, D.J., Struyven, R.R., Liu, T., Xu, M., Lozano, M.G., Woodward-Court, P., et al., 2023b. A foundation model for generalizable disease detection from retinal images. *Nature*, 1–8.